

Thermal conduction of carbon nanotubes using molecular dynamics

Zhenhua Yao*

*Singapore-MIT Alliance, National University of Singapore, Singapore 117576*Jian-Sheng Wang[†]*Department of Computational Science, National University of Singapore, Singapore 117543*

Baowen Li

*Department of Physics, National University of Singapore, Singapore 117542*Gui-Rong Liu[†]*Department of Mechanical Engineering, National University of Singapore, Singapore 119260*

(Received 29 December 2003; revised manuscript received 23 September 2004; published 24 February 2005)

The heat flux autocorrelation functions of carbon nanotubes (CNT's) with different radii and lengths are calculated using equilibrium molecular dynamics with periodic boundary conditions. The thermal conductance of CNT's is also calculated using the Green-Kubo formula from linear response theory. By pointing out an ambiguity in the cross-section definition of single-wall CNT's, we refer to the thermal conductance instead of conductivity in calculations and discussions. We find that the thermal conductance of CNT's diverges with the length of CNT's. After an analysis of vibrational density of states, it is shown that there are more and stronger low-frequency vibrational modes in longer CNT's, and these modes effectively contribute to the divergence of thermal conductance.

DOI: 10.1103/PhysRevB.71.085417

PACS number(s): 61.48.+c, 63.22.+m, 66.70.+f, 68.70.+w

I. INTRODUCTION

The carbon nanotube (CNT) was discovered by Iijima in 1991.¹ Since then, its unique mechanical, electrical, and optical properties have attracted intensive research activities on this quasi-one-dimensional material.² CNT's have high Young modulus and strength,³ as well as high thermal conductivity. Many novel applications in various areas have been proposed, including nanoscale electronic devices in the next generation electronic technologies.

As the dimensions of electronic devices shrink to the nanoscale, the thermal conduction problem becomes more and more important, as a significant amount of energy may be dissipated in a compact space. However, it is very difficult to measure the thermal conducting ability of nanoscale devices. Furthermore, the Fourier law, which describes the macroscopic thermal conduction phenomena, may not be appropriate for low-dimensional systems. Therefore, it is important to study the thermal conduction of nanoscale systems and to develop theoretical and computational methods for predicting the thermal properties of nanoscale materials and devices.

There are mainly two approaches to study theoretically the thermal conduction phenomena of nanoscale materials: the first is a macroscopic method using continuum models and kinetic theories, such as Boltzmann transport equation,^{4,5} and the second is a fundamental microscopic method based on first-principles atomistic simulations or quantum mechanical models. In the second approach, various methods are proposed to model the physical system and calculate the thermal conductivity. These methods include equilibrium and nonequilibrium molecular dynamics (MD) simulation as well as mode-coupling theory, etc.⁶ These methods study the

physical system from scratch and make little empirical assumptions.

The understanding of heat conduction and development of a complete theory are a long-standing and formidably difficult task. For insulating crystals, the problem of heat transportation by lattice vibrations is still far from being solved from some points of view. For mathematical simplicity, one-dimensional (1D) or two-dimensional lattices of atoms are naturally considered.⁶ This issue has been addressed for several decades. Recently, Li *et al.* established a connection between anomalous heat conduction and anomalous diffusion in one-dimensional systems,⁷ and Wang and Li studied the anomalous thermal conduction in 1D chains using MD and mode-coupling theory.⁸

In CNT's generally two physical mechanisms contribute to the thermal conduction: (i) electron-phonon interactions, which mainly depend on electronic band structures and the electron scattering process, etc., and (ii) phonon-phonon interactions, which depend on the vibrational modes of the lattice.

For semiconductor CNT's in room temperature, phonon-phonon interactions dominate the overall thermal conductivity and electron-phonon interactions have only a small contribution due to the large band gap and low density of free charge carriers.⁹ Fortunately the phonon-phonon contribution to thermal conduction can be well studied by classical MD.

The phonon mean free path in the axial direction of CNT's is estimated to be very long, from about 100 nm to 1 μm and much longer than that of other materials as well as the size of simulation domain; thus, the thermal conductivity of CNT's which are shorter than a few μm may have ballistic transport features.¹⁰ The finite size constrains the phonon motion and causes the thermal conductance to appear vari-

able with the CNT length. Actually, it is difficult to make the simulation domain larger than phonon mean free path even on supercomputers; thus, finding the “correct” value of thermal conductance remains a difficult task.

In the last few years, there have been many research activities on this subject. Berber *et al.* studied the thermal conductivity κ of CNT’s and the dependence of κ on temperature and suggested that κ is about 6600 W/mK for CNT (10,10) at room temperature.¹¹ Che *et al.* calculated the thermal conductivity of diamond materials and CNT’s, and showed that the theoretical value of thermal conductivity converges as the simulation system size increases. However, in their papers the errors of thermal conductivity values are too large to draw an accurate conclusion.¹² Maruyama¹⁰ studied the heat conduction in finite-length CNT’s using non-equilibrium MD and calculated the thermal conductivity from the measured temperature gradients and energy budgets in phantom molecules, and claimed that thermal conductivity of CNT (5,5) diverges as a power law, where the calculated size dependence of the thermal conductivity gave the power index 0.32. This result appears confirmed by Zhang and Li in study on anomalous heat diffusion.¹³ Osman and Srivastava found that κ shows a peaking behavior before falling off at higher temperatures due to the onset of umklapp scattering.¹⁴ Volz and Chen investigated the thermal conductivity of bulk silicon crystals based on MD simulation using Stillinger-Weber potential, and found that κ is independent of the length L_x of nanowire when L_x is larger than 16 lattice constants and the cross section area is smaller than a certain value.¹⁵

In addition to these theoretical studies there is some experimental work on the heat conduction of CNT’s. Yang *et al.* investigated the thermal conductivity of multiwall CNT’s using a pulsed photothermal reflectance technique and suggested that the effective κ could be about 200 W/mK.¹⁶ Kim *et al.* measured the thermal conductivity of a single CNT using a microfabricated suspended device and found that $\kappa > 3000$ W/mK at room temperature.¹⁷ Hone *et al.* measured the temperature-dependent thermal conductivity of crystalline ropes of single-wall CNT’s and argued that κ is dominated by phonons at all temperatures.¹⁸

In this work we use the Green-Kubo relation derived from linear response theory to examine the thermal conductance by calculating the heat flux autocorrelation functions. However, finite-size artifacts are still involved due to the frequency cutoff and the artificial autocorrelation introduced by periodic boundary conditions, which is consistent with the results of Volz and Chen.¹⁵ We find that the low-frequency vibrational modes of the lattice are limited by the size of simulation domain, and the thermal conductance of an infinite long CNT may be infinite.

II. COMPUTATION OF THERMAL CONDUCTIVITY USING MD

A. Green-Kubo relation and heat flux

In the macroscopic model of thermal conduction, the thermal conductivity is defined from the Fourier law which is for heat flow under a nonuniform temperature distribution. The

heat flux \mathbf{j} is related to the temperature gradient as $\mathbf{j} = -\kappa \nabla T$, where κ is the thermal conductivity tensor and T is the temperature distribution.

From the intuition of the Fourier law, a simple approach to study the thermal conduction of CNT’s is that, first, put the two ends in two heat reservoirs with different temperature (usually $T_0 + \Delta T$ and $T_0 - \Delta T$, where T_0 is supposed to be the average temperature of the system) and measure the heat flux along the axial direction and then calculate the thermal conductance. In simulations the heat flux should be collected after the system becomes steady, and a large number of averages over time is needed to get smooth temperature gradient curves and accurate heat flux data. However, the simulation domain which MD can efficiently handle is not large enough, and the temperature gradient due to a reasonable temperature difference of two heat reservoirs (note that too small a temperature difference gives a large error and poor results) is far too large to be realistic. Moreover, as the thermal conductance strongly depends on the temperature, results from the nonuniform temperature distribution may not be accurate. Schelling *et al.* systematically compared the equilibrium and nonequilibrium methods for computing the thermal conductivity of insulating materials¹⁹ and mentioned these problems. Moreover, if the thermal conductivity diverges with the tube length L , the divergence exponent β in $\kappa \propto L^\beta$ need not be the same for equilibrium and nonequilibrium simulations.²⁰

Due to the aforementioned reasons, in this work we use the fluctuation-dissipation theorem from linear response theory which connects the energy dissipation to the thermal fluctuations in the equilibrium state.^{5,21} In this method, the thermal conductivity in axial direction of CNT’s can be expressed in terms of heat flux autocorrelation function,^{5,21}

$$\kappa = \frac{1}{k_B T^2 V} \int_0^\infty \langle J(t)J(0) \rangle dt, \quad (1)$$

where $J(t) = \int \mathbf{j}(\mathbf{r}, t) dV$ is the total heat flux in the axial direction and V is the volume of the system. From the local energy balance equation

$$\frac{\partial \rho(\mathbf{r}, t)}{\partial t} + \nabla \cdot \mathbf{j}(\mathbf{r}, t) = 0, \quad (2)$$

where $\rho(\mathbf{r}, t)$ is the energy density (i.e., energy per unit volume)—and note that $\rho(\mathbf{r}, t)$ and $\mathbf{j}(\mathbf{r}, t)$ are macroscopic concepts—a microscopic expression for total heat flux can be derived as follows:

$$\mathbf{J}(t) = \frac{d}{dt} \sum_i \mathbf{r}_i(t) \epsilon_i(t), \quad (3)$$

where $\mathbf{r}_i(t)$ is the time-dependent coordinate of atom i . In MD simulations, the total potential energy can be divided among atoms; then, the site energy $\epsilon_i(t)$ can be taken to be

$$\epsilon_i = \frac{1}{2} m_i \mathbf{v}_i^2 + \frac{1}{2} \sum_j u(r_{ij}). \quad (4)$$

In the above equation, $u(r_{ij})$ is in fact a many-body potential,²² and the calculation of total heat flux $\mathbf{J}(t)$ is much

more complicated in this case than in case of using a simple pairwise potential function.

B. Interatomic potential

Currently there are several choices of potential functions for describing interatomic interactions in carbon materials: the Tersoff potential which was published in 1989 for the latest parameters,²² Brenner potential which was originally published in 1990²³ and revised in 2002,²⁴ environment-dependent interaction potential for carbon materials by Marks published in 2000,²⁵ and a new bond order potential in which parameters are fitted to tight-binding results.²⁶ In these potentials, the latter two have not been widely recognized. The Brenner potential with the latest parameters gives accurate results and is widely used. However, it is observed that in long-time microcanonical ensemble simulations,³⁵ the Brenner potential gives a larger total energy deviation than the Tersoff potential due to its complicated interpolation functions. The Tersoff potential is stable in long-time running according to our tests and gives fairly accurate results. Zheng *et al.*²⁷ compared Tersoff and Brenner potentials in their theoretical analysis of the thermal conduction of single-wall CNT's and got good results using both potentials, Berber has also used the Tersoff potential to study the thermal properties of CNT's and calculated the thermal conductivity.¹¹ Therefore, in our simulation we use the Tersoff potential. The Tersoff potential can be formally written as a summation of pairwise interactions,

$$V_{\text{tot}} = \frac{1}{2} \sum_{ij} f_c(r_{ij}) [V_R(r_{ij}) - B_{ij} V_A(r_{ij})], \quad (5)$$

where V_R and V_A are the repulsive and attractive parts of the potential, and their functional forms are given below:

$$V_R(r) = A \exp(-\lambda r), \quad V_A(r) = B \exp(-\mu r), \quad (6)$$

$$f_c(r) = \begin{cases} 1, & r < R, \\ \frac{1}{2} \left[1 + \cos \frac{\pi(r-R)}{S-R} \right], & R \leq r \leq S, \\ 0, & r > S, \end{cases} \quad (7)$$

where $f_c(r)$ is a cutoff function which explicitly restricts the interactions within the nearest neighbors and dramatically reduces the redundant computation in the force-potential evaluation procedure. In Eq. (5), B_{ij} is a bond order parameter and depends on the bonding environment around atom i and j . B_{ij} implicitly contains multibody information and thus the whole potential function is actually a multiple-body potential. The functional form of B_{ij} can be written as follows:

$$B_{ij} = [1 + (\beta \zeta_{ij})^n]^{-1/2n}. \quad (8)$$

The detailed information and parameters of Eqs. (5)–(8) are given in Tersoff's paper.²²

C. Finite-size effect

One of the major concerns in simulation of CNT's to calculate the thermal conductivity is the finite-size effect due to

periodic boundary conditions applied in the axial direction. As the simulation is conducted in a periodic box, the long-wavelength vibrational mode of the lattice is cut off while the CNT is short. This effect causes that a short CNT thermal conductivity is smaller than a long CNT thermal conductivity. Using MD, we investigate the thermal conductivity of CNT's with different lengths as well as the relationship between the thermal conductivity and the length, to study its convergence with system size.

It is noticed that with increasing CNT length more and stronger long-wavelength phonon modes are introduced to the system, and these modes are characterized by a longer mean free path (compare with a shorter CNT) and thus contribute more to the thermal conductance. Moreover, as a kind of quasi-1D material low-frequency modes play a more important part in heat conduction, as in 1D systems the acoustic vibrational density of states (VDOS) is a constant with k , while in 3D systems VDOS varies with k^2 where k is the wave vector. Taking into account this factor, the thermal conductance depends on the size of the system. Although it was demonstrated that in some 3D systems the thermal conductivity is also size dependent,³¹ for CNT's the thermal conductance should be much stronger size dependent, and for infinite CNT's it remains unknown whether the thermal conductance converges or not.

D. Thermal conductance vs thermal conductivity

It should be mentioned here that since an isolated single-wall CNT cross section can be defined in different ways, its thermal conductivity has also arbitrary definitions and is not a well-defined quantity. Some definitions of the cross section A of single-wall CNT's are as follow.

(i) Consider the CNT as a solid cylinder; then, the cross section area will be πR^2 , where R is the radius of the CNT.

(ii) Consider the CNT as a hollow cylinder; then, the cross section area will be $2\pi R\delta$, where δ is the thickness of CNT shell. In the literature usually two values of δ are used: one is 3.4 Å, which is the interlayer distance of graphite materials; the other is 1.42 Å, which is the length of sp^2 bond.

Therefore, in the literature many different values of thermal conductivity are reported; some of them mainly differ in the cross-section definition.

Obviously, the definition of the cross section is not important for the thermal conduction research of CNT's, as we only need to calculate and compare the results consistently. However, for comparing different results from different research groups, this arbitrariness must be eliminated. In this work, we use the quantity of "thermal conductance" $\kappa' = \kappa A$, which equals the thermal conductivity times cross-section area. Thus, the thermal conductance has the dimension of "W m/K." Note that even in experiment, what can be measured is heat power (energy per unit time) and temperature gradient, the ambiguity of the CNT cross section also enters.

E. Simulation procedure

In this work, CNT's with different sizes are investigated. First, armchaired CNT's (10,10) with different lengths are

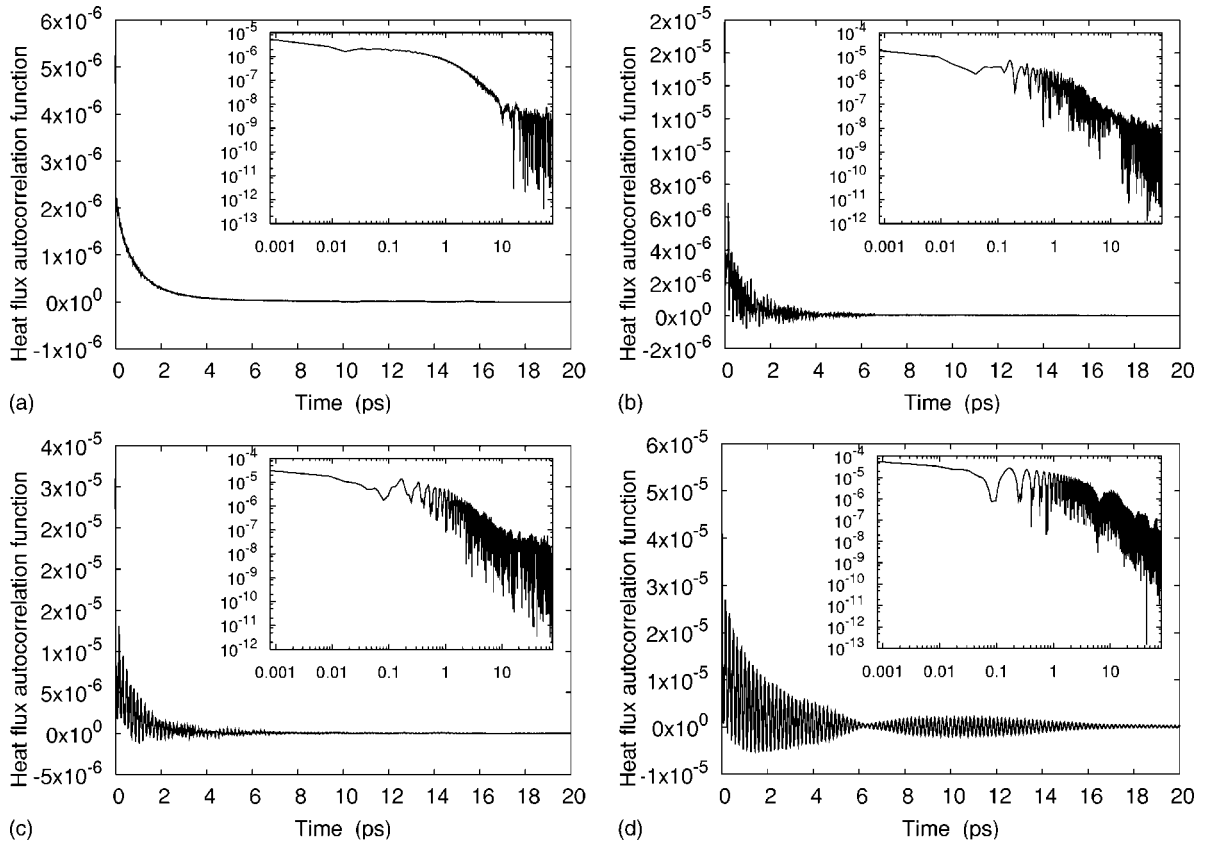


FIG. 1. Initial heat flux autocorrelation function (0–20 ps) of CNT (10, 10) with 50, 100, 200, and 400 layers, respectively (from left to right, top to bottom). Insets are log-log curves of full time range.

simulated; then, CNT (15,15) and (5,5) are simulated. In our MD simulation program, the time integration algorithm is implemented by using the velocity Verlet method. For improving the computation performance, a new neighbor list algorithm using cell decomposition is employed.²⁸ In all simulation cases, a periodic boundary condition is used only in the axial direction of CNT's. For each simulation case, we carry out the following three steps.

(i) First, canonical ensemble MD is running for 10^5 – 5×10^5 steps in order to take the average system temperature to 300 K and wait until system reaches thermal equilibrium.

(ii) Then it is followed by microcanonical ensemble running for another 10^5 – 5×10^5 steps and wait until system reaches a thermal equilibrium in the new ensemble.

(iii) Finally microcanonical ensemble MD continues to run and heat flux data are calculated and collected in every time step. After every 10^5 steps, the power spectra of heat flux data are online calculated; meanwhile, its arithmetic average and Fourier transform, which is heat flux autocorrelation function, as well as the statistical errors are calculated and dumped to disk files.

In this work, the last step runs indefinitely and stops until accurate results are obtained after many times of average. Generally 10^8 steps were carried out in this step. In other words, about 1000 averages have been done to obtain the final data. The total amount of CPU time is about 3 months on 10 Pentium III 866MHz PCs and three dual-CPU Alpha EV67/667MHz workstations.

In MD simulation, time step is 0.8 fs, and the canonical ensemble simulation is implemented by a Noé-Hoover algorithm.²⁹

III. RESULTS AND DISCUSSIONS

Figure 1 shows the autocorrelation function of the total heat flux along the axial direction of CNT (10,10) with 50, 100, 200, and 400 layers. A very sharp decay in the beginning followed by a very slow decay can be seen clearly. An oscillation in the autocorrelation function can also be seen in the curves, and it becomes larger when the CNT is longer. The oscillation is related to the low-frequency phonon mode in the system³² and becomes stronger as the length of the CNT increases. From Fig. 2 it can be seen that the frequency of the autocorrelation oscillation is only related to the chiral index of CNT's, not to the length of CNT's. The value of autocorrelation function increases as the CNT length increases. The fast initial decay is believed to be contributed by high-frequency vibrational modes in the CNT, and slow decay is contributed by low-frequency modes which have a much longer wavelength.

The insets of Fig. 1 are the log-log curves of the heat flux autocorrelation function. Note that data points in the range of 8–80 ps are in the order of 10^{-7} – 10^{-8} and are almost random errors. The origin of these errors are mainly due to inaccurate velocity trajectories and roundoff errors in floating operations. Data points in the range of 0.001–0.8 ps cor-

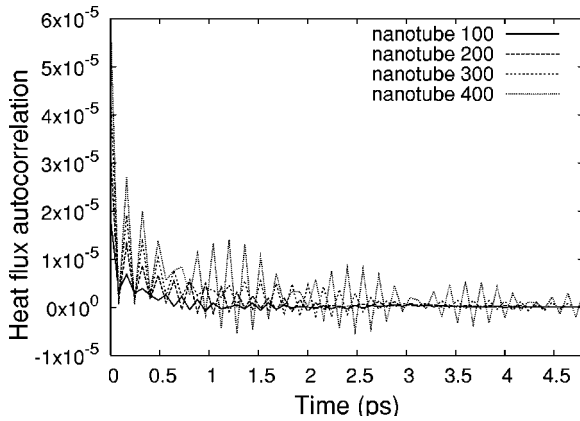


FIG. 2. Initial decay of heat flux autocorrelation function of CNT (10,10) with 100, 200, 300, and 400 layers, respectively.

respond to initial decay in the very early moment and the number of points is small (though this section seems quite long in the graph); thus, the middle section in the range of 0.8–8 ps should show asymptotic behavior. And it can be seen that roughly the correlation function decays as a power law $f(t) \approx ct^\alpha$. Theoretically, we expect $\alpha = -d/\delta$ where d is the dimension and δ is the exponent related to the decay of modes (see the Appendix).

From data in the insets of Fig. 1 we calculate the power index α of the heat flux autocorrelation function decay using the linear least-squares method (data after 8 ps are not used due to too large errors) and show the relationship between α and the length of CNT in Fig. 3. From the Green-Kubo formula,⁶ knowledge of the asymptotic behavior of $\langle \mathbf{J}(t)\mathbf{J}(0) \rangle$ allows the determination of the dependence of the thermal conductance on the system size N . From Fig. 3 it can be seen that the power index of the heat flux autocorrelation function decay is about $-3/2$, and for certain cases it is near -1 ; thus, the thermal conductance κ' should converge to a finite value as the system size increases, on the basis of this exponent. However, when the length of CNT's is between 50 and 600 layers in our work, there is no evidence that κ will converge. Strangely, this fast growth of the thermal conductance with sizes appears mainly from contributions at short times.

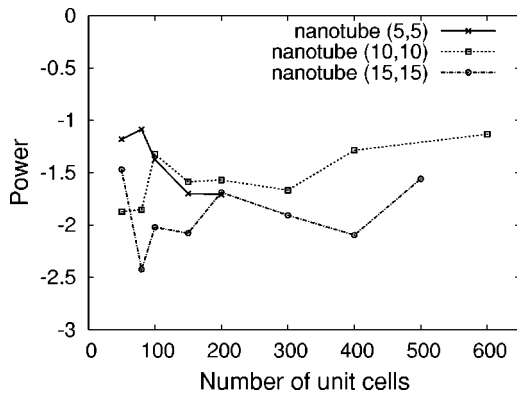
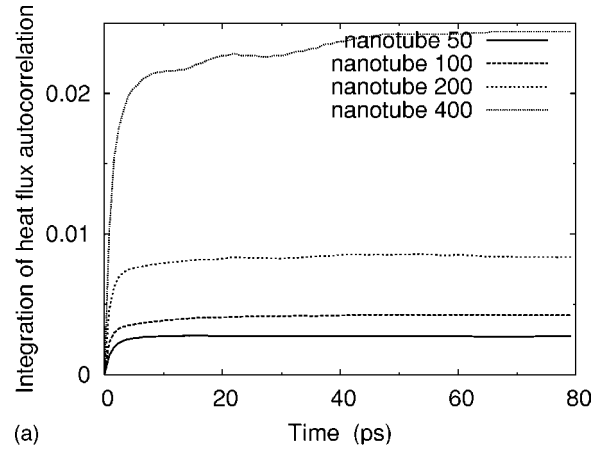
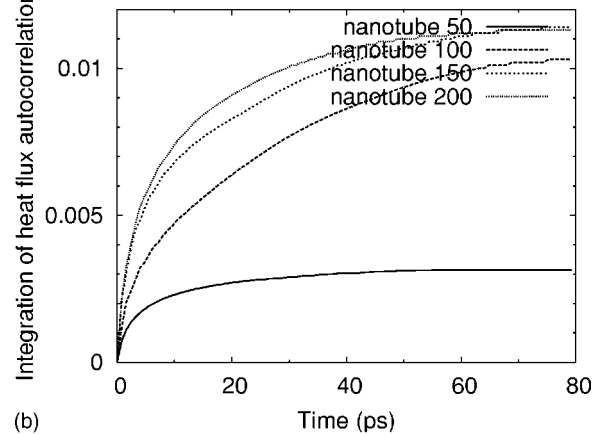


FIG. 3. Relationship between decay power index and length of CNT (5,5), (10,10), and (15,15). (Power indices for shorter CNT's have also smaller errors.)



(a)



(b)

FIG. 4. Integration of the heat flux autocorrelation function over time t up to given number of time steps for CNT (10,10) (top) and (5,5) (bottom).

The curves shown in Fig. 4 are the integration of the heat flux autocorrelation function over time t . It can be seen that both the initial fast decay and long-time slow decay contribute to the thermal conductance. The cutoff of long-wavelength vibrational modes will significantly influence the final result of the thermal conductivity. Compared with CNT (10,10), the integration of the heat flux autocorrelation function for CNT (5,5) converges more slowly, especially for the longer CNT's. The integration of heat flux autocorrelation function for CNT (15,15) is qualitatively similar to CNT (10,10), and it converges fast, so we do not show it in Fig. 4.

As discussed in Sec. II D, the absolute thermal conductivity value of an isolated single-wall CNT is ambiguous because the cross section is not well defined, so we discuss only the thermal conductance. The relationship between the thermal conductance and the length of CNT is shown in Fig. 5 in logarithmic scale. In all cases, the thermal conductance of the single-wall CNT does not converge to a finite value as the length of the CNT increases. In the figure we also give the standard errors of thermal conductance results and mark in the error bars. The error is calculated as follows.

(i) In microcanonical ensemble simulations, N_{tot} number of time steps is carried out; thus, N_{tot} heat flux data points are collected.

(ii) Divide these heat flux data to N groups, each group

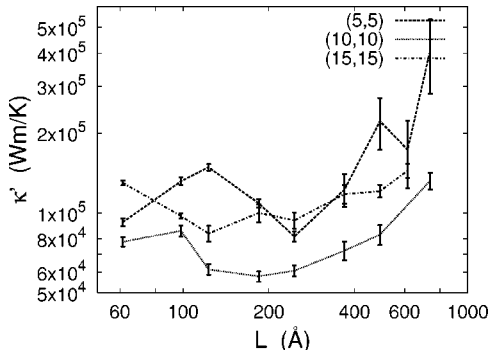


FIG. 5. Thermal conductance as a function of the CNT length. In the graph solid line, dotted line, and dashed line denote the thermal conductance of CNT (5,5), (10,10), and (15,15), respectively.

has M heat flux data points, and calculate the heat flux auto-correlation function and integration for each group, respectively.

(iii) The final result is taken to be the average of N groups of results in the second step. Meanwhile, the standard error of the result is given by

$$S_i = \sqrt{\frac{1}{N} \sum_{j=1}^M (\xi_j - \bar{\xi})^2}, \quad i = 1, \dots, N.$$

From Fig. 5 it can be seen that as long as the length of the CNT increases, the thermal conductance increases correspondingly, and this trend has been discovered in the literature.¹⁰ If we consider the van der Waals thickness 3.4 Å as the thickness of the CNT shell and treat the CNT as a hollow cylinder, the thermal conductivity results are in good agreement with Maruyama's data.¹⁰ From Fig. 6 we also notice that as the length of the CNT, L , increases, κ'/L (where κ' is the thermal conductance) tends to a constant [except perhaps the (5,5) case]. If this result can be confirmed, then it means that thermal conduction is ballistic in the region of our model parameters studied and the length of the CNT is the mean free path.

In order to understand why a longer CNT has higher thermal conductance, we calculate the VDOS by computing the power spectrum of the velocity correlation function while the

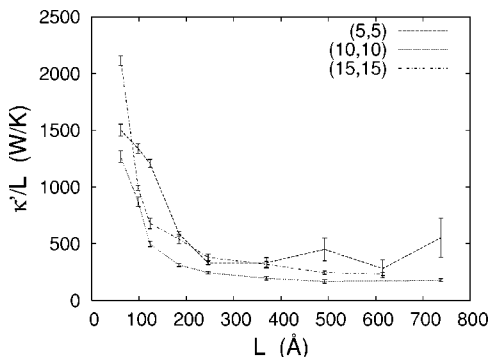


FIG. 6. Thermal conductance divided by the length of the CNT with the function of L .

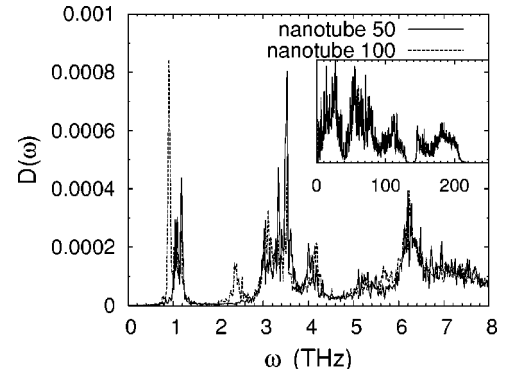


FIG. 7. Vibrational density of states of CNT (10,10) with 50 and 100 layers, respectively. The inset shows the VDOS in the full frequency range, and the full graph shows the VDOS in the low-frequency range. In the graphs, the dashed lines denote the VDOS of the CNT with 100 layers and the solid line denotes the VDOS of the CNT with 50 layers.

simulation is running, and the calculation can be expressed as follows:³⁰

$$D_z(\omega) = \int \exp(-i\omega t) \langle v_z(t) v_z(0) \rangle dt, \quad (9)$$

where $D_z(\omega)$ denotes the VDOS along the z axis (i.e., the axial direction) and $v_z(t)$ denotes the velocity of atoms in the z axis. Figure 7 shows the VDOS of CNT's with 50 and 100 layers, respectively. The inset of Fig. 7 shows the VDOS of two CNT's in the full frequency range, and it seems that two curves are almost the same; this indicates that the middle- and high-frequency distributions of VDOS of two CNT's are roughly identical. In order to verify the VDOS calculation using MD, phonon modes of CNT (10,10) unit cell are calculated using the density functional theory generalized gradient approximation (DFT-GGA) and the linear response theory,^{33,34} and the results show that the lowest mode is about 1.379 THz and the highest mode is about 294.9 THz. The results are in good agreement with MD calculations, except that anharmonic effect is of course ignored and different length CNT's have the same vibrational modes in principle. However, from the graph of low-frequency range, it can be seen that the CNT with 100 layers has more low frequency vibration modes; this is why a longer CNT has a higher thermal conductance. We believe that the CNT with 100 layers has a larger simulation domain, has a longer phonon mean free path, and then has more low-frequency modes.

IV. CONCLUSIONS

In this paper the high thermal conductance of single-wall CNT's is calculated using equilibrium MD, and the relationship between thermal conductance and length of the CNT is discussed. It is found that as a kind of quasi-one-dimensional material, the CNT thermal conductance does not converge to a finite value as the CNT length increases up to 80 nm. It can also be seen that a longer CNT has more long wavelength vibrational modes, and these modes contribute to the thermal

conduction as the CNT is longer. The specific form of divergence (the exponent) needs further investigation.

ACKNOWLEDGMENTS

This project is supported by the Singapore-MIT Alliance. The authors thank Dr. Gang Zhang for discussion and Dr. Min Cheng for revising the manuscript. The authors thank Dr. Sebastian Volz of Ecole Centrale Paris for giving us comments and a note on the thermal conductivity of CNT's (mainly in the Appendix).

APPENDIX: A SIMPLE EXPLANATION TO THE THERMAL CONDUCTIVITY OF CNT'S

From the mode-coupling theory it is known that the decay behavior of the heat flux autocorrelation function is related to the convergence of the thermal conductivity with the length of carbon CNT's. In this section, a simple derivation is given to explain this relationship. In this paper the analysis of the thermal conductivity of CNT's starts from the Green-Kubo formula [see Eq. (1)]. The heat flux can be decomposed into modes,

$$JV = \sum_k \hbar \omega_k v_{gk} \delta n_k(t), \quad (\text{A1})$$

where ω_k is the mode frequency, v_{gk} represents the mode group velocity, and δn_k is the deviation of the phonon number from equilibrium. Combining this expression in the Green-Kubo equation and neglecting the cross terms, we have

$$\langle J(0)J(t) \rangle = \frac{1}{V^2} \sum_k (\hbar \omega v_g)^2 \langle \delta n_k(0) \delta n_k(t) \rangle. \quad (\text{A2})$$

If we model the phonon autocorrelation by an exponentially decaying function $\langle \delta n_k(0) \delta n_k(t) \rangle = \langle \delta n_k(0)^2 \rangle e^{-t/\tau_k}$ and consider that $\langle \delta n_k(t)^2 \rangle = \langle n_k(t)^2 \rangle$ and the phonon number can be written as $\langle \delta n_k(0)^2 \rangle = \langle n_k(0)^2 \rangle = (k_B T / \hbar \omega)^2$, then we have

$$\langle J(0)J(t) \rangle = \frac{(k_B T)^2}{V^2} \sum_k v_{gk}^2 e^{-t/\tau_k}. \quad (\text{A3})$$

If the discrete sum over the modes on the right-hand side of the above equation is turned into a continuous integral, we

integrate on the volume V_{rs} occupied by the CNT modes in reciprocal space:

$$\sum_k v_{gk}^2 e^{-t/\tau_k} = \int_{V_{rs}} v_g^2 e^{-t/\tau_k} d^3k. \quad (\text{A4})$$

Generally $d^3k \sim k^{d-1} dk$, where d is the dimension of the structure. The integral can also be done in the frequency domain using the dispersion relation $k \propto \omega$. This means that the dimension d is given by the power law at low frequency of the phonon density of states.

The basic assumption is that the decay constant τ_k is some power of k , $\tau_k \propto k^\delta$. Now set a simple variable change $u = t c k^\delta$, where δ is the power law of the spectral relaxation time. Equation (A3) can be changed to

$$\begin{aligned} \langle J(0)J(t) \rangle &= \left(\frac{k_B T}{V} \right)^2 \int_k k^{d-1} e^{t c k^\delta} d|k| \\ &= \left(\frac{k_B T}{V} \right)^2 \frac{1}{\delta (t c)^{d/\delta}} \int_u u^{d/\delta-1} e^{-u} du \\ &\sim t^{-d/\delta}. \end{aligned} \quad (\text{A5})$$

Note that the integration of $\langle J(0)J(t) \rangle$ is proportional to the thermal conductivity; then, if $d \neq \delta$,

$$\int_0^\infty t^{-d/\delta} dt = \frac{1}{-d/\delta+1} t^{-d/\delta+1} \Big|_0^\infty, \quad (\text{A6})$$

and if $d = \delta$,

$$\int_0^\infty t^{-1} dt = \ln(t) \Big|_0^\infty. \quad (\text{A7})$$

Note that the limit $t=0$ is not physical so that the divergence at this limit should not be considered.

From the above derivation it can be seen that if $d/\delta < 1$, the thermal conductivity of the infinitely long CNT is also infinite.

*Electronic address: yaozhenhua@yahoo.com

†Also in Singapore-MIT Alliance, National University of Singapore, Singapore 117576.

¹S. Iijima, *Nature (London)* **354**, 56 (1991).

²M. S. Dresselhaus, G. Dresselhaus, and R. Saito, *Carbon* **33**, 883 (1995); J. W. Mintmire and C. T. White, *ibid.* **33**, 893 (1995).

³Z. Yao, C.-C. Zhu, M. Cheng, and J. Liu, *Comput. Mater. Sci.* **22**, 180 (2001).

⁴S. Harris, *An Introduction to the Theory of the Boltzmann Equa-*

tion (Holt, Rinehart and Winston, New York, 1971); E. M. Lifshitz and L. P. Pitaevskii, *Physical Kinetics* (Pergamon Press, Oxford, New York, 1981).

⁵R. Kubo, M. Toda, and N. Hashitsume, *Statistical Physics* (Berlin, Springer, 1985), Vol. 2.

⁶S. Lepri, R. Livi, and A. Politi, *Phys. Rep.* **377**, 1 (2003).

⁷B. Li, L. Wang, and B. Hu, *Phys. Rev. Lett.* **88**, 223901 (2002); B. Li, G. Casati, and J. Wang, *Phys. Rev. E* **67**, 021204 (2003);

B. Li and J. Wang, *Phys. Rev. Lett.* **91**, 044301 (2003); B. Li, G.

- Casati, J. Wang, and T. Prosen, *ibid.* **92**, 254301 (2004).
- ⁸J.-S. Wang and B. Li, Phys. Rev. Lett. **92**, 074302 (2004); Phys. Rev. E **70**, 021204 (2004).
- ⁹B. T. Kelly, *Physics of Graphite* (Applied Science, New Jersey, 1981).
- ¹⁰S. Maruyama, Physica B **323**, 193 (2002).
- ¹¹S. Berber, Y.-K. Kwon, and D. Tománek, Phys. Rev. Lett. **84**, 4613 (2000).
- ¹²J. Che, T. Çağın, and W. A. Goddard III, Nanotechnology **11**, 65 (2000); J. Che, T. Çağın, W. Deng, and W. A. Goddard III, J. Chem. Phys. **113**, 6888 (2000).
- ¹³G. Zhang and B. Li, cond-mat/0403393 (unpublished).
- ¹⁴M. A. Osman and D. Srivastava, Nanotechnology **12**, 21 (2001).
- ¹⁵S. G. Volz and G. Chen, Phys. Rev. B **61**, 2651 (2000); Appl. Phys. Lett. **75**, 2056 (1999).
- ¹⁶D. J. Yang, Q. Zhang, G. Chen, S. F. Yoon, J. Ahn, S. G. Wang, Q. Zhou, Q. Wang, and J. Q. Li, Phys. Rev. B **66**, 165440 (2002).
- ¹⁷P. Kim, L. Shi, A. Majumdar, and P. L. McEuen, Phys. Rev. Lett. **87**, 215502 (2001).
- ¹⁸J. Hone, M. Whitney, C. Piskoti, and A. Zettl, Phys. Rev. B **59**, R2 514 (1999).
- ¹⁹P. K. Schelling, S. R. Phillpot, and P. Keblinski, Phys. Rev. B **65**, 144306 (2002).
- ²⁰J. M. Deutsch and O. Narayan, Phys. Rev. E **68**, 010201(R) (2003); **68**, 041203 (2003).
- ²¹A. J. C. Ladd, B. Moran, and W. G. Hoover, Phys. Rev. B **34**, 5058 (1986).
- ²²J. Tersoff, Phys. Rev. B **39**, 5566 (1989).
- ²³D. W. Brenner, Phys. Rev. B **42**, 9458 (1990).
- ²⁴D. W. Brenner, O. A. Shenderova, J. A. Harrison, S. J. Stuart, B. Ni, and S. B. Sinnott, J. Phys.: Condens. Matter **14**, 783 (2002).
- ²⁵N. A. Marks, Phys. Rev. B **63**, 035401 (2000).
- ²⁶D. G. Pettifor and I. I. Oleinik, Phys. Rev. B **59**, 8487 (1999); I. I. Oleinik and D. G. Pettifor, *ibid.* **59**, 8500 (1999).
- ²⁷Q. Zheng, G. Su, J. Wang, and H. Guo, Eur. Phys. J. B **25**, 233 (2002).
- ²⁸Z. Yao, J.-S. Wang, G. Liu, and M. Cheng, Comput. Phys. Commun. **161**, 27 (2004).
- ²⁹S. Noše, Mol. Phys. **52**, 255 (1984); W. G. Hoover, Phys. Rev. A **31**, 1695 (1985).
- ³⁰S. Muto and H. Aoki, J. Phys.: Condens. Matter **12**, L83 (2000).
- ³¹C. Herring, Phys. Rev. **95**, 954 (1954).
- ³²A. J. H. McGaughey and M. Kaviani, Phys. Rev. B **69**, 094303 (2004).
- ³³The results have been obtained through the use of the ABINIT code, a common project of the Universite Catholique de Louvain, Corning Incorporated, and other contributors (URL: <http://www.abinit.org>).
- ³⁴X. Gonze, J.-M. Beuken, R. Caracas, F. Detraux, M. Fuchs, G.-M. Rignanese, L. Sindic, M. Verstraete, G. Zerah, F. Jollet, M. Torrent, A. Roy, M. Mikami, Ph. Ghosez, J.-Y. Raty, and D. C. Allan, Comput. Mater. Sci. **25**, 478 (2002); X. Gonze, Phys. Rev. B **55**, 10 337 (1997); X. Gonze and C. Lee, *ibid.* **55**, 10 355 (1997).
- ³⁵We run over 10^8 steps, as a large number of steps is needed for obtaining accurate heat flux autocorrelation function data in our work.